Parametric Reconstruction of Kinetic PET Data with Plasma Function Estimation

Mustafa E. Kamasak[a], Charles A. Bouman[a], Evan D. Morris[b] and Ken Sauer[c]

[a]School of Electrical and Computer Engineering, Purdue University, West Lafayette, IN;
[b]Indiana University, Purdue University-Indianapolis Radiology and Biomedical Engineering Departments, Indianapolis, IN;
[c]Department of Electrical Engineering, University of Notre Dame, Notre Dame, IN;

ABSTRACT

It is often necessary to analyze the time response of a tracer. A common way of analyzing the tracer time response is to use a compartment model and estimate the model parameters. The model parameters are generally physiologically meaningful and called "kinetic parameters". In this paper, we simultaneously estimate both the kinetic parameters at each voxel and the model-based plasma input function directly from the sinogram data. Although the plasma model parameters are not our primary interest, they are required for accurate reconstruction of kinetic parameters. The plasma model parameters are initialized with an image domain method to avoid local minima, and multiresolution optimization is used to perform the required reconstruction. Good initial guesses for the plasma parameters are required for the algorithm to converge to the correct answer. Therefore, we devised a preprocessing step involving clustering of the emission images by temporal characteristics to find a reasonable plasma curve that was consistent with the kinetics of the multiple tissue types. We compare the root mean squared error (RMSE) of the kinetic parameter estimates with the measured (true) plasma input function and with the estimated plasma input function. Tests using a realistic rat head phantom and a real plasma input function show that we can simultaneously estimate the kinetic parameters of the two-tissue compartment model and plasma input function. The RMSE of the kinetic parameters increased for some parameters and remained the same or decreased for other parameters.

Keywords: tomography, input function estimation, iterative reconstruction, dynamic PET, kinetic modeling

1. INTRODUCTION

The tracer concentration in the plasma, also called input function, is required for the estimation of physiological parameters. This plasma concentration is generally obtained by sampling blood from arteries and direct measurement of activity in these samples.[1] However, there are many risks associated with this invasive procedure such as arterial thrombosis, arterial sclerosis, and irreversible tissue ischemia. Furthermore, the arterial sampling causes discomfort to the patients and may expose the medical staff to additional radiation. As a result of these drawbacks, there has been growing interest to develop algorithms that eliminate the need for arterial blood sampling. Gunn *et al.*[2] proposed a reference region model. In this model, the brain is segmented into target (with specific binding) and reference (no specific binding) regions. An expression for the input function in terms of kinetic parameters can be obtained from the reference region in the brain, and this expression can be substituted in the target region to eliminate the need for plasma concentrations. Takikawa *et al.*,[3] Onishi *et al.*,[4] and Eberl *et al.*[5] proposed population-based methods. The arterial sample measurements obtained from a population of former patients were used to approximate the input function. This approach is validated for $[^{18}F]$fluorodeoxyglucose (FDG) in positron emission tomography (PET),[5] and $[^{123}I]$iomazenil in single-photon emission computed tomography (SPECT).[4] Litton,[6] Chen *et al.*,[7] and Liptrot *et al.*[8] proposed image-derived

Send correspondence to Mustafa E. Kamasak
Mustafa E. Kamasak: E-mail: kamasak@purdue.edu, Telephone: +1 765 496 3717
Charles A. Bouman: E-mail: bouman@ecn.purdue.edu, Telephone: +1 765 494 0340
Evan D. Morris: E-mail: emorris@iupui.edu, Telephone: +1 317 274 1802
Ken Sauer: E-mail: sauer@nd.edu, Telephone: +1 574 631 6999

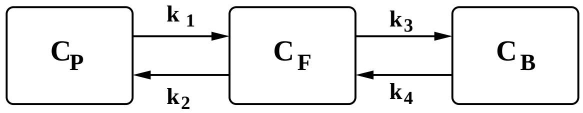

Figure 1. 2 tissue compartment model with 4 kinetic parameters.

input function estimation. In these cases, the input function is estimated from imaged volumes that consist primarily of blood. Morris *et al.*,[9] used a shape-based method to derive the input function by automatically identifying voxels that were mostly like to represent the blood signal in perfusion MR images. Feng *et al.*[10] and Wong *et al.*[11] estimated a model-based input function and kinetic parameters simultaneously from the images.

Recently, we have proposed a method to estimate the kinetic parameters directly from PET sinograms using parametric iterative coordinate descent (PICD).[12] We also showed that for simulated data the PICD method can improve over image domain estimation methods. As with image domain estimation methods, PICD algorithm requires the arterial input function to be known. In this paper, we extend the idea of direct reconstruction from sinograms to include the estimation of a model-based plasma input function. The scale of the plasma input function and tracer uptake rate cannot be estimated individually. Because a linear increase in the plasma concentration or tracer uptake rate produces the same measurements. Therefore, we fixed the scale of the plasma input function and estimate the tracer uptake rate within an unknown scale factor. With this extension, the PICD algorithm can be used in the cases where the input function is not known.

This paper is organized as follows; Section 2 reviews the 2-tissue compartment model and the set of ODE's that govern a tracer's kinetics. Section 3 introduces the PICD algorithm for direct parametric reconstruction. Section 4 presents simulation results. Conclusion follows the results.

2. TWO-TISSUE COMPARTMENT MODEL

Compartment models are commonly used in modelling physiological processes.[13] A compartment model is characterized by the number of its compartments and their interactions. Each compartment in a model represents a distinct physical space or different states of the tracer. In this paper, we used a 2-tissue compartment model with 4 parameters. This model is commonly used to describe the uptake and retention of an analog of glucose, 2-deoxy-2-[^{18}F]fluoro-D-glucose (FDG). The model can also be properly applied to receptor ligand studies provided that there is no non-specific binding and that the tracer has been administered at sufficiently high specific activity. Figure 1 illustrates the model: C_P (pmol/ml) is the molar concentration of tracer in the plasma, C_F (pmol/ml) is the molar concentration of unbound tracer, and C_B (pmol/ml) is the molar concentration of metabolized or bound tracer. The model depends on the kinetic parameters, k_1, k_2, k_3, and k_4, which specify the tracer exchange rates between compartments in units of inverse minutes. The parameters k_1, k_2, and k_4 are first order rate constants, and k_3 is an *apparent* first order rate constant describing a process (metabolism or receptor-binding) that proceeds in proportion to the concentration of the labelled tracer only, as long as the number of sites available for binding do not become rate-limiting.

In addition to the above-stated parameters, there are two compound parameter groups that have ready physiological interpretations and practical application, particularly for receptor-ligand imaging: binding potential (BP), and total volume of distribution (VD). BP is proportional to the number of receptors and VD represents the steady state distribution of tracer between the plasma and tissue. BP and VD can be expressed in terms of the aforementioned kinetic parameters,

$$BP = \frac{k_3}{k_4} \tag{1}$$

$$VD = \frac{k_1}{k_2}\left(1 + \frac{k_3}{k_4}\right) . \tag{2}$$

In applying the model in Fig. 1 to all voxels, we assume that the delivery of tracer is the same to all regions being imaged. In other words, the value of C_P is not a function of voxel position. However, the values of the kinetic parameters will be allowed to vary for each voxel location, s.

Forward Transforms	Inverse Transforms
$a_s = \frac{k_{1s}}{2\Delta}(k_{2s} - k_{3s} - k_{4s} + \Delta)$	$k_{1s} = a_s + b_s$
$b_s = \frac{k_{1s}}{2\Delta}(-k_{2s} + k_{3s} + k_{4s} + \Delta)$	$k_{2s} = \frac{a_s c_s + b_s d_s}{a_s + b_s}$
$c_s = \frac{1}{2}(k_{2s} + k_{3s} + k_{4s} + \Delta)$	$k_{3s} = \frac{a_s b_s (c_s - d_s)^2}{(a_s + b_s)(a_s c_s + b_s d_s)}$
$d_s = \frac{1}{2}(k_{2s} + k_{3s} + k_{4s} - \Delta)$	$k_{4s} = \frac{c_s d_s (a_s + b_s)}{a_s c_s + b_s d_s}$
$\Delta = \lvert\sqrt{(k_{2s} + k_{3s} + k_{4s})^2 - 4k_{2s}k_{4s}}\rvert$	

Table 1. Forward and inverse transformations from standard kinetic parameters $[k_{1s}, k_{2s}, k_{3s}, k_{4s}]$ for the voxel s to new parameters $[a_s, b_s, c_s, d_s]$. Note that $c_s = \alpha_2$ and $d_s = \alpha_1$ given in equation 8.

In this work, the plasma concentration, C_P, is modelled using 5 parameters[14] as

$$C_P(\phi, t) = \{(A_1(t-\tau) - A_2)e^{-\lambda_1(t-\tau)} + A_2 e^{-\lambda_2(t-\tau)}\}u(t-\tau) \ , \tag{3}$$

where $\phi = [A_1, A_2, \lambda_1, \lambda_2, \tau]^t$ is the array of plasma model parameters, and $u(\cdot)$ is the unit step function. Using these assumptions, the time variation of the concentrations for a single voxel are governed by the following ordinary differential equations (ODE).

$$\frac{dC_F(s,\phi,t)}{dt} = k_{1s}C_P(\phi,t) - (k_{2s} + k_{3s})C_F(s,\phi,t) + k_{4s}C_B(s,\phi,t) \tag{4}$$

$$\frac{dC_B(s,\phi,t)}{dt} = k_{3s}C_F(s,\phi,t) - k_{4s}C_B(s,\phi,t) \ . \tag{5}$$

The solution to the ODE's in (4,5) is given by

$$C_F(s,\phi,t) = \left\{\frac{k_{1s}}{\alpha_2 - \alpha_1}[(k_{4s} - \alpha_1)e^{-\alpha_1 t} + (\alpha_2 - k_{4s})e^{-\alpha_2 t}]u(t)\right\} * C_P(\phi,t) \tag{6}$$

$$C_B(s,\phi,t) = \left\{\frac{k_{1s}k_{3s}}{\alpha_2 - \alpha_1}[e^{-\alpha_1 t} - e^{-\alpha_2 t}]u(t)\right\} * C_P(\phi,t) \tag{7}$$

where $*$ indicates continuous-time convolution, and

$$\alpha_1, \alpha_2 = \frac{(k_{2s} + k_{3s} + k_{4s}) \mp \sqrt{(k_{2s} + k_{3s} + k_{4s})^2 - 4k_{2s}k_{4s}}}{2} \ . \tag{8}$$

where α_1 and α_2 are real valued constants that result from the subtraction and addition of terms in (8) respectively.

Next, we transform the kinetic parameters (k_1, k_2, k_3, k_4) to form the new parameters (a, b, c, d) as shown in Table 1. This transformation is important because while the parameters (a, b, c, d) are well suited for optimization, (k_1, k_2, k_3, k_4) are more physiologically relevant. We use $\varphi_s = [a_s, b_s, c_s, d_s]^t$ to denote the parameter vector for each voxel s.

The total activity concentration (e.g., in nCi/ml) for voxel s at time t is denoted by

$$\begin{aligned} f(\varphi_s,\phi,t) &\triangleq (1 - V_B)\left[C_F(s,\phi,t) + C_B(s,\phi,t)\right] S_A e^{-\lambda t} + V_B C_{WB}(t) \\ &= (1 - V_B)\left[(a_s e^{-c_s t} + b_s e^{-d_s t})u(t) * C_P(\phi,t)\right] S_A e^{-\lambda t} + V_B C_{WB}(t) \end{aligned} \tag{9}$$

where S_A is the initial specific activity of the tracer (nCi/pmol), λ is the decay rate of the isotope (min^{-1}), V_B is a known constant for the volume fraction of the voxel that contains blood, and C_{WB} (nCi/ml) is the tracer activity concentration in whole blood (i.e., plasma plus blood cells plus other particulate matter). *

*Notice that both $f(\varphi_s, t)$ and $C_{WB}(t)$ in equation (9) include decay, either explicitly or implicitly. Therefore, the sinogram data should not be decay corrected for the implementation of this method.

We next discretize $f(\varphi_s, \phi, t)$ using $t_0, \cdots, t_{K-1}$ as the K discrete times at which the tissue is imaged. The activity at each time for voxel s is given by the $1 \times K$ row vector

$$f(\varphi_s, \phi) = [f(\varphi_s, \phi, t_0), f(\varphi_s, \phi, t_1), \cdots, f(\varphi_s, \phi, t_{K-1})] \ . \tag{10}$$

Let the N voxels be indexed by the values $s = 0, 1, \cdots, N-1$, and let $\varphi = [\varphi_0, \varphi_1, \cdots, \varphi_{N-1}]$ denote the $4 \times N$ matrix of parameters at all voxels. With this, we define the $N \times K$ function

$$F(\varphi, \phi) = \begin{bmatrix} f(\varphi_0, \phi) \\ \vdots \\ f(\varphi_{N-1}, \phi) \end{bmatrix}$$

which maps the parametric image, φ, to the activity of each voxel at each time. Finally, let $F(\varphi, \phi, t_k)$ denote the k^{th} column of $F(\varphi, \phi)$, so $F(\varphi, \phi, t_k)$ contains the activity for each voxel at time t_k.

3. PARAMETRIC RECONSTRUCTION FROM SINOGRAM DATA WITH PLASMA FUNCTION ESTIMATION

In this section, we describe our method for reconstructing the parametric image, φ, and estimating the plasma function directly from sinogram data. We do this by first formulating a conventional scanner model under the assumption that the sinogram measurements are Poisson random variables. We then use the kinetic model of Section 2 as the input to the scanner model. Once the complete forward model is formulated, we present a cost function that consists of a negative log likelihood and a prior for the kinetic parameters. The reconstructed kinetic parameters are essentially the maximum *a posteriori* (MAP) estimate of the kinetic parameters, but they are computed by simultaneously optimizing the plasma model parameters, ϕ, along with the kinetic parameters. This algorithm can also be viewed as joint MAP estimation with a uniform prior distribution for the plasma model parameters.[15] Although the plasma model parameters are not of direct interest, they are required for the accurate reconstruction of kinetic parameters.

3.1. Scanner Model

Let Y_{mk} denote the sinogram measurement for projection $0 \leq m < M$ and time frame $0 \leq k < K$, and let Y be the $M \times K$ matrix of independent Poisson random variables that form the sinogram measurements. Furthermore, let A be the forward projection matrix, with elements A_{ms} (counts-ml/nCi), and let μ be the number of accidental coincidences. Then the expected number of counts for each measurement at a given time, t_k is given by

$$E[Y_{mk}|F(\varphi, \phi, t_k)] = \sum_{s=0}^{N-1} A_{ms} f(\varphi_s, \phi, t_k) + \mu \ . \tag{11}$$

This relationship can be compactly expressed using matrix notation as

$$E[Y|F(\varphi, \phi)] = AF(\varphi, \phi) + \mu \ . \tag{12}$$

It is easily shown that under these assumptions the probability density for the sinogram matrix is given by[16]

$$p(Y|\varphi, \phi) = \prod_{k=0}^{K-1} \prod_{m=0}^{M-1} \frac{(A_{m*}F(\varphi, \phi, t_k) + \mu)^{Y_{mk}} e^{-(A_{m*}F(\varphi, \phi, t_k) + \mu)}}{Y_{mk}!} \tag{13}$$

where A_{m*} is the m^{th} row of the system matrix, A. The log likelihood of the sinogram matrix is then given by

$$LL(Y|\varphi, \phi) = \sum_{k=0}^{K-1} \sum_{m=0}^{M-1} Y_{mk} \log(A_{m*}F(\varphi, \phi, t_k) + \mu) - (A_{m*}F(\varphi, \phi, t_k) + \mu) - \log(Y_{mk}!) \ . \tag{14}$$

This is a very general formulation. For specific scanners, the form of the system matrix A may vary considerably, and accurate determination of the matrix A can be critical to obtaining accurate tomographic reconstructions.[17]

$$
\begin{array}{l}
\text{foreach iteration } \{ \\
\qquad \hat{\varphi} \leftarrow \arg\min_{\varphi} C(Y|\varphi, \phi) \\
\qquad \hat{\phi} \leftarrow \arg\min_{\phi} C(Y|\hat{\varphi}, \phi) \\
\}
\end{array}
$$

Figure 2. Each iteration of optimization has two steps; first the plasma model parameters were kept fixed and parametric image is updated, then plasma model parameters are estimated for the updated parametric image.

3.2. Estimation Framework

For the joint optimization of the kinetic parameters and the plasma model parameters, a cost function is formed by negating the log likelihood given in (14) and adding a stabilizing function.

$$C(Y|\varphi, \phi) = -LL(Y|\varphi, \phi) + S(\varphi) \tag{15}$$

The kinetic parameter reconstructions and the plasma model parameters can be estimated by minimizing this cost function;

$$\{\hat{\varphi}, \hat{\phi}\} \leftarrow \arg \min_{\{\varphi, \phi\}} C(Y|\varphi, \phi)\ . \tag{16}$$

The stabilizing function can be obtained from an assumed prior probability distribution for the parametric image. In this work, we model the distribution of the parametric image as a Markov random field (MRF) with a Gibbs distribution of the form

$$p(\varphi) = \frac{1}{z} \exp\{- \sum_{\{s,r\} \in \mathcal{N}} g_{s-r} \|T(\varphi_s) - T(\varphi_r)\|_W^q\} \tag{17}$$

where z is the normalization constant, $\mathcal{N}$ is the set of all neighboring voxel pairs in φ, g_{s-r} is the coefficient linking voxels s and r, q is a constant parameter that controls the smoothness of the edges in the parametric image, $T(\cdot)$ is a transform function, and W is the diagonal weighting matrix.

In this paper, we will assume $q = 2$ and that $\mathcal{N}$ is formed with voxel pairs using an 8-point neighborhood system. In this case, the probability density function corresponds to a Gaussian Markov random field, and we choose the negative logarithm of this function as our stabilizing function.

$$S(\varphi) = \sum_{\{s,r\} \in \mathcal{N}} g_{s-r} \|T(\varphi_s) - T(\varphi_r)\|_W^2\ . \tag{18}$$

By choosing an appropriate transform function, $T(\cdot)$, the regularization can be done in the space of the physiologically relevant parameters. Typically, we will select $T(\cdot)$ to transform from the a, b, c, d space to the k_1, k_2, k_3, k_4 as shown in Table 1; however, any well behaved one-to-one transformation, $T(\cdot)$, is suitable for our algorithm.

3.3. Optimization Strategy using PICD

Simultaneous update of the parametric image, φ, and plasma model parameters, ϕ, is not tractable. Therefore, we chose an iterative optimization strategy. Each iteration had two steps; 1) estimate the kinetic parameters using parametric iterative coordinate descent (PICD) algorithm[12] by keeping the plasma model parameters constant, 2) update the plasma model parameters (See Fig. 2).

The PICD algorithm is similar to the ICD algorithm used in conventional PET image reconstruction,[16] but it is adapted to account for the nonlinear parameters of the compartmental model. PICD sequentially updates the parameters of each voxel thereby monotonically decreasing the cost function given in Equation (16);

$$\varphi_s \leftarrow \arg \min_{\varphi_s} C(Y|\varphi_s, \varphi)\ . \tag{19}$$

When $F(\varphi, \phi)$ is a nonlinear function, the PICD algorithm reduces computation by decoupling the dependencies between the compartment model nonlinearities and the forward tomography model. Therefore, it is computationally efficient.

After updating the parametric image, the plasma model parameters are sequentially updated using line searches;

$$
\begin{aligned}
\hat{A}_2 &\leftarrow \arg\min_{A_2} C(Y|\varphi, [A_1, A_2, \lambda_1, \lambda_2, \tau]) \\
\hat{\lambda}_1 &\leftarrow \arg\min_{\lambda_1} C(Y|\varphi, [A_1, \hat{A}_2, \lambda_1, \lambda_2, \tau]) \\
\hat{\lambda}_2 &\leftarrow \arg\min_{\lambda_2} C(Y|\varphi, [A_1, \hat{A}_2, \hat{\lambda}_1, \lambda_2, \tau]) \\
\hat{\tau} &\leftarrow \arg\min_{\tau} C(Y|\varphi, [A_1, \hat{A}_2, \hat{\lambda}_1, \hat{\lambda}_2, \tau]) \\
\hat{\phi} &\leftarrow [A_1, \hat{A}_2, \hat{\lambda}_1, \hat{\lambda}_2, \hat{\tau}]
\end{aligned}
$$

Note that in equation (4) k_{1s} and $C_P(\phi, t)$ are multiplied. We can estimate the value of $k_{1s}C_P(\phi, t)$, but we cannot individually estimate the scale of the plasma concentration and tracer uptake rate, k_{1s}. In our optimization framework, the scale of the plasma function is determined by A_1 and A_2, and the scale of the tracer uptake rate is a function of a_s and b_s. Therefore, only three parameters out of A_1, A_2, a_s, and b_s can be identified at the same time. In order to address this unidentifiability issue, A_1 can be fixed to a constant, and in this case, parameters A_2, k_1 and VD can only be estimated within a scale factor. Other parameters (k_2, k_3, k_4, and BP) are not effected. It may be possible to use some additional experimental data such as injected dosage or a single late blood sample or prior information such as population-average blood curve to properly scale the plasma input function (A_1 and A_2) and the kinetic parameters (k_1 and VD).[18]

3.4. Initialization

The joint estimation strategy described in Section 3.3 can converge to local minimum with an arbitrary initial plasma input function. To avoid local minima, a good initial plasma input function is required. In order to choose good initial plasma model parameters, we used an approach similar to Feng *et al.*[10] (See fig. 3.) First, we reconstructed the sinograms using filtered back projection (FBP). The voxels were then segmented into a pre-determined number of clusters according to their reconstructed time responses.[19] Each cluster was represented by a single time response. Let L be the number of clusters, and x_l be the representative time response of cluster l. Then, initial plasma model parameters and the kinetic parameters for each cluster were chosen to minimize the weighted least squares between the time responses of the clusters and the model;

$$\{\varphi_0^{init}, \cdots, \varphi_{L-1}^{init}, \phi^{init}\} \leftarrow \arg \min_{\{\varphi_0, \cdots, \varphi_{L-1}, \phi\}} \sum_{l=0}^{L-1} \|x_l - f(\varphi_l, \phi)\|_{W_l}^2 \ . \tag{20}$$

In this equation, W_l denotes the $K \times K$ diagonal weighting matrix for cluster l. W_l is formed by the inverses of the time-response variances, i.e. the k^{th} diagonal element of W_l is given by

$$[W_l]_{k,k} = \frac{\Delta t_k}{x_{l,k}} \ ,$$

where Δt_k is the duration of the k^{th} time frame, and $x_{l,k}$ is the time response of cluster l at time t_k. Note that, this initialization may also converge to a local minimum. However, it is a relatively fast method, and it can be executed many times starting from different points. The solution that minimizes equation (20) can be chosen as the initial point for our algorithm.

It is well known that for the tomographic problem the ICD reconstruction algorithm tends to have slow convergence at low spatial frequencies.[20] To solve this problem, we use a multiresolution reconstruction scheme, which first computes coarse resolution reconstructions and then proceeds to finer scales. The coarsest resolution reconstruction is initialized with ϕ^{init} and a single set of parameters obtained by weighted least squares curve

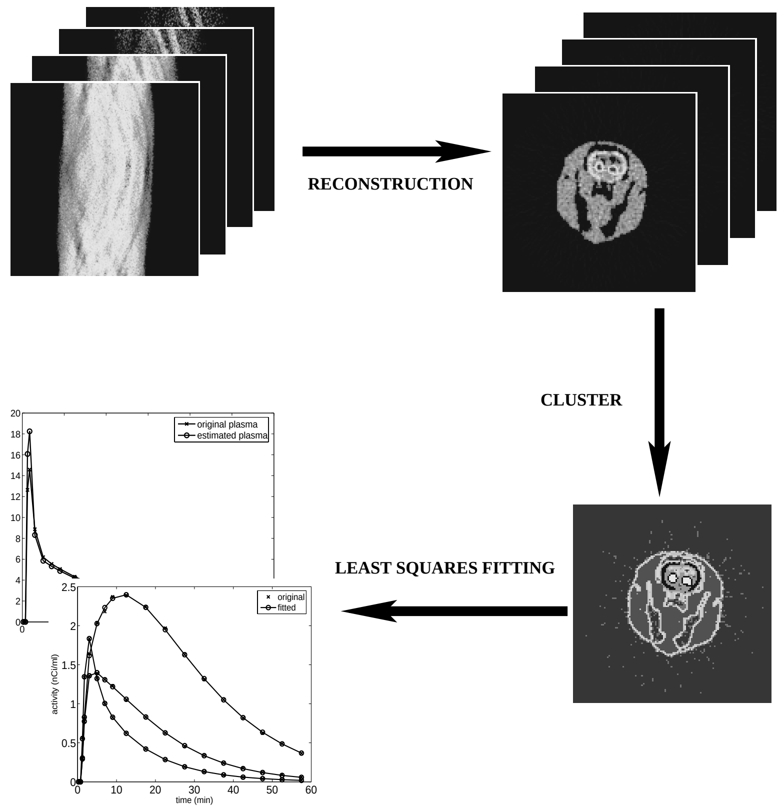

Figure 3. Initialization strategy for plasma model parameters. First sinograms are reconstructed, then the tomographic reconstructions are clustered. Finally plasma model parameters and kinetic parameters are estimated using least squares curve fitting.

fitting to the average emission rate of each time frame. Importantly, the average activity of each time frame can be calculated directly from the sinogram data with little computation. Finer resolution reconstructions are then initialized by interpolating the parametric reconstruction of the previous coarser resolution. This recursive process reduces computation because the computationally inexpensive reconstructions at coarse levels provide a good initialization for finer resolution reconstructions.

4. SIMULATION AND RESULTS

The following section compares the accuracy of kinetic parameter estimates with measured plasma input function, and with estimated plasma input function.

4.1. Phantom Design

Our simulation experiments are based on a phantom of a rat's head. Figure 4(a) shows a schematic representation of the rat phantom and its constituent regions. The phantom has 7 regions including the background. These regions were obtained by segmenting an MRI scan of a rat through automated and manual techniques.[21] The regions and their corresponding parameters[22] are given in Table 2, and their time activity curves are shown in Fig. 4(b). Time frames of emission images are generated using these parameter images and the 2-tissue compartment model equations. The plasma function, $C_P(t)$, is obtained by arterial plasma sampling of a rat scanned in IndyPET-II.[23] The blood contribution to the PET activity is assumed to be zero, and the tracer is assumed to be raclopride with ^{11}C, which has a decay constant of $\lambda = 0.034$ min^{-1}. Total scan time is 60 min., divided into 18 time frames with 4×0.5 min, 4×2 min, and 10×5 min. The phantom had a resolution of 128×128 with each voxel having dimensions of (1.2 mm)^3.

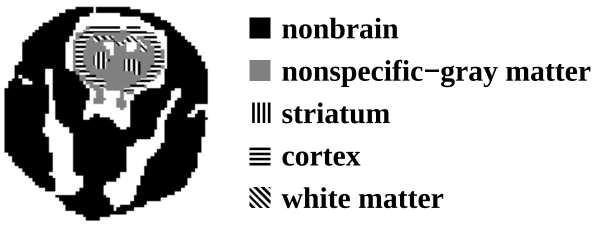

(a)

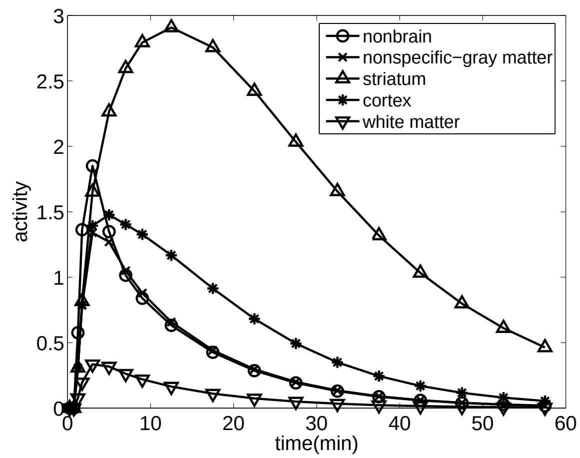

(b)

Figure 4. (a) Regions of the rat phantom derived from a segmented MR Image. (b) Time-activity curves for 5 distinct tissue regions in rat brain phantom.

Region	k_1 min^{-1}	k_2 min^{-1}	k_3 min^{-1}	k_4 min^{-1}	a min^{-1}	b min^{-1}	c min^{-1}	d min^{-1}
Background	0	0	0	0	0	0	0	0
CSF	0	0	0	0	0	0	0	0
Nonbrain	.1836	.8968	0	0	.1836	0	.8968	0
Nonspecific-gray matter	.0918	.4484	0	0	.0918	0	.4484	0
Striatum	.0918	.4484	1.2408	.1363	.02164	.07016	1.7914	.0312
Cortex	.0918	.4484	.141	.1363	.0607	.0311	.628	.09725
White matter	.02295	.4484	0	0	.02295	0	.4484	0

Table 2. Kinetic parameters used in the simulations for distinct tissue regions of the rat head.

The rat phantom image at each time frame is forward projected into a sinogram using a Poisson model for the detected counts with a background (accidental coincidence) level of 0.001 nCi/ml. Each sinogram consists of 180 angles and 200 radial bins per angle. A triangular point spread function with a 4 mm base width is used in forward projections.

4.2. Algorithmic Implementation

The plasma model parameters were initialized as described in Section 3.4. Since we cannot identify A_1,A_2 and k_1 simultaneously, we can fix A_1 to any arbitrary value. However, with an arbitrary A_1 the estimated values of A_2, k_1 and VD will be off by a scale factor. We fixed A_1 to its true value.

In the initialization, the tomographic reconstructions are clustered into 8 regions. To find initial plasma model parameters, 10 starting points in the range of $2 \leq A_2 \leq 10$, $0.5 \leq \lambda_1 \leq 5$, $0 \leq \lambda_2 \leq 0.2$, $0 \leq \tau \leq 2$ were used, and for each of these the solution that minimizes equation (20) is chosen as the initial point.

The maximum likelihood (ML) estimate of the stabilizing function parameters were computed from true parametric image and used in the simulations.[24]

The kinetic parameters are reconstructed using PICD algorithm with three levels of multiresolution optimization corresponding to resolutions 32×32, 64×64, and 128×128. Regularization was applied directly to the k_1, k_2, BP, and VD parameters. The multiresolution PICD method was executed with a fixed number of iterations at each resolution; 40 iterations at 32×32 resolution, 20 iterations at 64×64 resolution, and 10 iterations at 128×128 resolution.

	true	estimated
A_1	49.325	–
A_2	7.310	7.341
λ_1	1.789	1.617
λ_2	0.045	0.045
τ	0.893	0.825

Table 3. True and estimated plasma model parameters. Note that A_1 is not estimated.

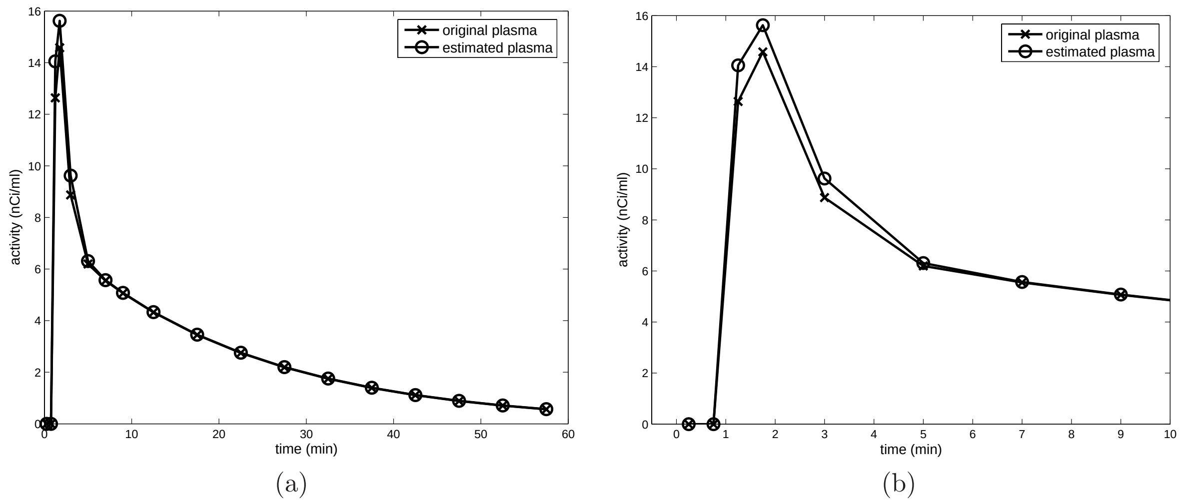

Figure 5. (a) Measured and estimated plasma input functions (b) Measured and estimated plasma function in the first 10 minutes.

4.3. Results

Table 3 shows the true and estimated plasma model parameters. Figure 5(a) shows the measured (true) plasma input function and estimated plasma input function, and Fig. 5(b) displays only the first 10 min of the measured and estimated plasma input functions.

Figure 6 and 7 display the kinetic parameter reconstructions with the measured plasma input function and with the estimated plasma input function. All kinetic parameters in these figures are estimated with regularization on k_1, k_2, BP, and VD.

Figure 8 shows the normalized RMSE of the kinetic parameter estimates, k_2, k_3, k_4, and BP with the measured and estimated plasma input function. Note that these are the only kinetic parameters that we can estimate without any side information. The RMSE of parameters k_2 and k_3 are calculated over the support of k_1, and the RMSE of k_4 is calculated over the support of k_3.[†] From this figure, the RMSE of k_2, and k_4 estimates increase with estimated plasma input function.

5. CONCLUSION AND FUTURE WORK

We have demonstrated that it is possible to estimate kinetic parameters k_2, k_3, k_4, and BP directly from the PET sinograms without plasma input function measurements. The tracer uptake rate, k_1, and VD can only be estimated to within a scale factor since the scale of the plasma input function is not known. A model-based plasma input is estimated jointly with kinetic parameters. In our simulation, with real plasma input function and realistic phantom, the estimated plasma input function was close to the measured (true) input function.

[†]When k_1 is zero, then k_2 and k_3 are not defined. Similarly, when k_3 is zero, k_4 is not defined.

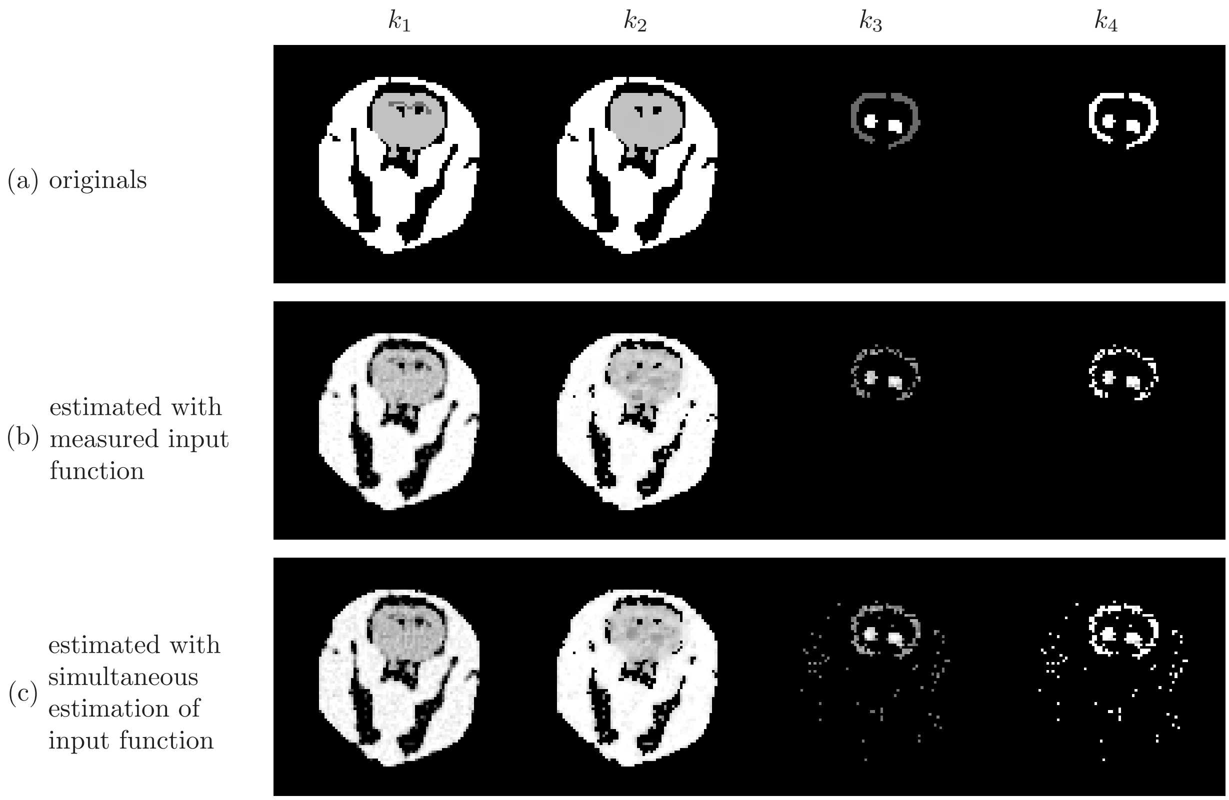

Figure 6. (a) Original k_1, k_2, k_3, and k_4. Estimated k_1, k_2, k_3, and k_4 (b) estimated with measured input function, and (c) estimated with simultaneous estimation of input function.

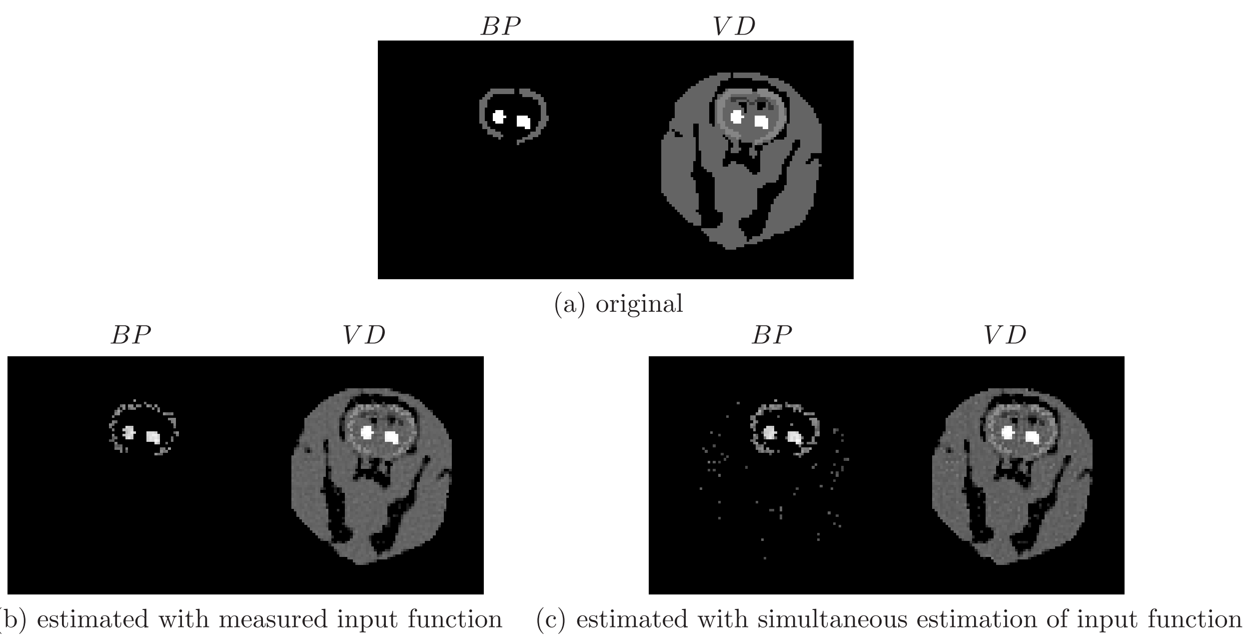

Figure 7. Original BP and VD. Estimated BP and VD (b) estimated with measured input function, and (c) estimated with simultaneous estimation of input function.

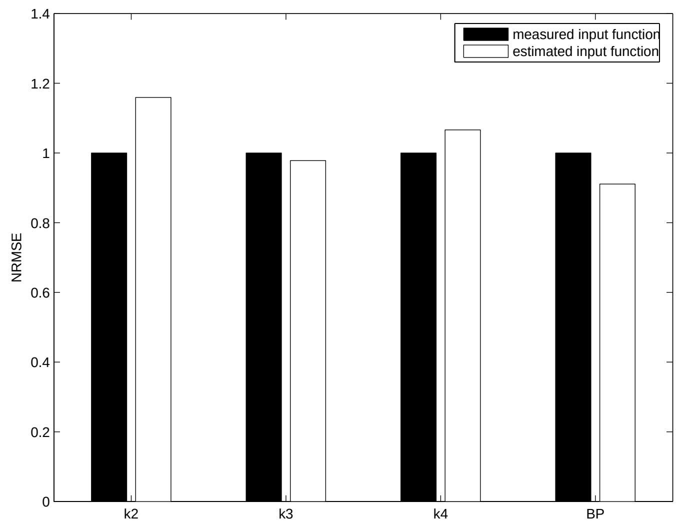

Figure 8. Normalized RMSE of the kinetic parameter estimations with measured input function and with estimated input function.

Furthermore, some of the estimated kinetic parameters have higher RMSE (k_2 and k_4), some of them (k_3 and BP) have either similar or lower RMSE when the input function is estimated.

Better optimization for plasma model parameters may also be needed for avoiding local minima and for computational efficiency. Further simulations and tests with real data are needed to analyze the the RMSE, bias, and variance of the kinetic parameter estimations.

Acknowledgement

Authors would like to thank Cristian Constantinescu, Chunzhi Wang, Dr. Karmen Yoder and Dr. Ti-Qiang Li at Indiana University School of Medicine for their help in constructing the rat phantom from MR data.

REFERENCES

1. M. E. Phelps, J. C. Maziotta, and H. R. Schelbert, *Positron Emission Tomography and Autoradiography, Principles and Applications for the Brain and Heart*, ch. 7. Raven Press, Raven Press, 1140 Avenue of the Americas, New York, NY 10036, 1986.
2. R. N. Gunn, A. A. Lammertsma, S. P. Hume, and V. J. Cunningham, "Parametric imaging of ligand-receptor binding in PET using a simplified reference region model," *NeuroImage* **6**(4), pp. 279–287, 1997.
3. S. Takikawa, V. Dhawan, P. Spetsieris, W. Robeson, T. Chaly, R. Dahl, D. Margouleff, and D. Eidelberg, "Noninvasive quantitative fluorodeoxyglucose PET studies with and estimated input function derived from a population-based arterial blood curve," *Radiology* **188**, pp. 131–136, 1993.
4. Y. Onishi, Y. Yonekura, S. Nishizawa, F. Tanaka, H. Okazawa, K. Ishiza, T. Fujita, J. Konishi, and T. Mukai, "Noninvasive quantification of iodine-123-iomazenil SPECT," *Journal of Nuclear Medicine* **37**(2), pp. 374–378, 1996.
5. S. Eberl, A. R. Anayat, R. R. Fulton, P. K. Hooper, and M. J. Fulham, "Evaluation of two population-based input functions for quantitative neurological FDG PET studies," *Eur. J. Nucl. Med.* **24**(3), pp. 299–304, 1997.
6. J.-E. Litton, "Input function in PET brain-studies using MRI defined arteries," *J. Comp. Ass. Tom.* **21**(6), pp. 907–909, 1997.
7. K. Chen, D. Bandy, E. Reiman, S. C. Huang, M. Lawson, D. Feng, L. Yun, and A. Palant, "Noninvasive quantification of the cerebral metabolic rate for glucose using positron emission tomography, 18F-fluoro-2deoxyglucose, the patlak method, and an image-derived input function," *J. Cereb. Blood Flow Metab.* **18**(7), pp. 716–723, 1998.

8. M. Liptrot, K. H. Adams, L. Martiny, L. H. Pinborg, M. N. Lonsdale, N. V. Olsen, S. Holm, C. Svarer, and G. M. Knudsen, "Cluster analysis in kinetic modelling of the brain: a noninvasive alternative to arterial sampling," *NeuroImage* **21**(2), pp. 483–493, 2004.
9. E. D. Morris, J. W. Vanmeter, T. A. Tasciyan, J. M. Maisog, and T. A. Zeffiro, "Automated determination of the arterial input function for quantitative MR perfusion analysis," in *Proc. Intl. Soc. Magn. Reson. Med.*, p. 740, 2000.
10. D. Feng, K.-P. Wong, C.-M. Wu, and W.-C. Siu, "A technique for extracting physiological parameters and the required input function simultaneously from PET image measurements: Theory and simulation study," *IEEE Transactions on Information Technology in Biomedicine* **1**, pp. 243–254, December 1997.
11. K.-P. Wong, D. Feng, S. R. Meikle, and M. J. Fulham, "Simultaneous estimation of physiological parameters and the input function - in *vivo* PET data," *IEEE Transactions on Information Technology in Biomedicine* **5**, pp. 67–76, March 2001.
12. M. Kamasak, C. A. Bouman, E. D. Morris, and K. Sauer, "Direct reconstruction of kinetic parameter images from dynamic PET data," in *Proceedings of 37th Asilomar Conference on Signals, Systems and Computers*, pp. 1919–1923, (Pacific Grove, CA), November 9-12 2003.
13. E. D. Morris, C. J. Endres, K. C. Schmidt, B. T. Christian, R. F. M. Jr., and R. E. Fisher, "Kinetic modeling in PET," in *Emission Tomography: The Fundamentals of PET and SPECT*, M. Wernick and J. Aarsvold, eds., ch. 23, Academic Press, San Diego, 2004.
14. D. Feng, S.-C. Huang, and X. Wang, "Models for computer simulation studies of input functions for tracer kinetic modeling with positron emission tomography," *International Journal of Biomedical Computing* **32**(2), pp. 95–110, 1993.
15. A. Mohammad-Djafari, "Joint estimation of parameters and hyperparameters in a Bayesian approach of solving inverse problems," in *Proc. of IEEE Int'l Conf. on Image Proc.*, **II**, pp. 473–476, (Lausanne, Switzerland), September 16-19 1996.
16. C. A. Bouman and K. Sauer, "A unified approach to statistical tomography using coordinate descent optimization," *IEEE Trans. on Image Processing* **5**, pp. 480–492, March 1996.
17. E. Mumcuoglu, R. M. Leahy, S. Cherry, and E. Hoffman, "Accurate geometric and physical response modeling for statistical image reconstruction in high resolution PET scanners," in *Proceedings of IEEE Nuclear Science Symposium and Medical Imaging Conference*, pp. 1569–1573, 1996.
18. G. J. Hunter, L. M. Hamberg, N. M. Alpert, N. C. Choi, and A. J. Fischman, "Simplified measurement of deoxyglucose utilization rate," *Journal of Nuclear Medicine* **37**(6), pp. 950–955, 1996.
19. K.-P. Wong, D. Feng, S. R. Meikle, and M. J. Fulham, "Segmentation of dynamic PET images using cluster analysis," *IEEE Trans. on Nuclear Science* **49**(1), pp. 200–207, 2002.
20. K. Sauer and C. A. Bouman, "A local update strategy for iterative reconstruction from projections," *IEEE Trans. on Signal Processing* **41**, pp. 534–548, February 1993.
21. G. Paxinos and C. Watson, *The Rat Brain in Stereotaxic Coordinates*, Academic Press, 4th ed., 1998.
22. S. Pappata, S. Dehaene, J. B. Poline, M. C. Gregoire, A. Jobert, J. Delforge, V. Frouin, M. Bottlaender, F. Dolle, L. D. Giamberardino, and A. Syrota, "In vivo detection of striatal dopamine release during reward: a PET study with [^{11}C]raclopride and a single dynamic scan approach," *Neuroimage* **16**(4), pp. 1015–1027, 2002.
23. N. C. Rouze, K. M. Stantz, and G. D. Hutchins, "Design of indyPET-II, a high-resolution, high-sensitivity dedicated research scanner," in *Proceedings of Nuclear Science Symposium Conference*, pp. 1545–1549, 2001.
24. S. S. Saquib, C. A. Bouman, and K. Sauer, "ML parameter estimation for Markov random fields with applications to Bayesian tomography," *IEEE Trans. on Image Processing* **7**, pp. 1029–1044, July 1998.